This is a preprint, the final version is subject to change, of the American Mineralogist (MSA)
Cite as Authors (Year) Title. American Mineralogist, in press.
(DOI will not work until issue is live.) DOI: http://dx.doi.org/10.2138/am.2014.4571

Revision 1 of MS #4571

Chemistry of bone mineral, based on the hypermineralized rostrum of the beaked whale *Mesoplodon densirostris*

ZHEN LI AND JILL D. PASTERIS*

Department of Earth and Planetary Sciences, Washington University in St. Louis, St. Louis, MO, 63130, U.S.A.

ABSTRACT

Carbonate-substituted hydroxylapatite is the inorganic component in bone. The nanometer size of bone crystallites and their interweaving with subequal volumes of collagen fibrils make the chemical analysis of the bone mineral extremely difficult. The few available chemical analyses commonly were made on ashed bone, which, in addition to mineral, also includes chemical residues of collagen. For the present study, we chose the rostrum of the whale *Mesoplodon densirostris*. Its mineral content of up to 96 wt% makes it an ideal material for pursuing the chemistry of bioapatite within bone. Both bulk (X-ray fluorescence, thermogravimetry, and carbon analysis) and point analyses and element mapping (electron microprobe) were applied to this densest of bone materials. Its bioapatite has an average carbonate content of ~8 wt% and an average Ca/P atomic ratio of 1.7. The rostrum shows extremely low-concentration trace elements (Al, Si, Fe, Ti and Sr) and some minor elements (K and Cl) as in typical bone materials. Homogeneity of elemental distribution is demonstrated in typical mineral-dominated areas within the rostrum sections except around a few vascular holes and vessels. The very good correlation between electron microprobe point analyses and the XRF bulk analyses of the rostrum indicate the latter to be a useful chemical model of bone mineral. The bulk analysis shows that the bioapatite in the rostrum has an average composition of $(Ca_{8.40}Mg_{0.20}Na_{0.54})[(PO_4)_{4.87}(CO_3)_{1.13}]\ (OH)_{0.87}$.

Key words: Apatite, bone, whale rostrum, electron microprobe, X-ray fluorescence

INTRODUCTION

The hydroxylapatite (OHAP), $Ca_{10}(PO_4)_6(OH)_2$, member of the apatite group is a relatively rare occurrence geologically (Mitchell et al., 1943; Pan and Fleet, 2002), but it is the basis of all

biological forms of apatite. Bioapatite is a carbonate-containing variety of OHAP, which forms the inorganic component of bone, tooth enamel, and tooth dentin, (Glimcher, 1959; 1962; LeGeros et al., 1969; McConnell, 1970; Biltz and Pellegrino, 1977; LeGeros, 1981; Rey et al., 1989; Elliott, 1994; Elliott, 2002; Rey et al., 2007b). Despite the importance of bone mineral in the biomechanics of bone (Currey, 1979) and the chemical equilibrium in the body (Biltz et al., 1981), the exact chemistry of bone apatite has not been fully defined.

A typical bone, e.g., human femur, consists of ~55 wt% mineral, ~35 wt% collagen, and 15 wt% water (Rogers and Zioupos, 1999). Mineral therefore is the most abundant component within bone. However, the bone mineral crystallites are nanometer in scale, and they are intimately interwoven with collagen fibrils (Glimcher, 1959; Currey, 2002; Rey et al., 2007a). Because of the analytical challenge posed by the nanocomposite we call bone, relatively few chemical analyses of major (Ca, P, and O) and minor (Na, Mg, S, F, Cl, and K) elements of bone and bone mineral have been reported in the literature since the 1980s (LeGeros, 1981; Driessens, 1982; LeGeros and LeGeros, 1984; Zioupos et al., 2000; Elliott, 2002; Skinner, 2005). Moreover, most of the reported chemical compositions were not obtained on the actual mineral crystallites, but rather on the residues of bone (referred to as bone ash), i.e., after heating to at least 500 ^{o}C (LeGeros and LeGeros, 1984). Such residues may contain ions from ashed collagen as well as from the original mineral. The published chemical data are based mainly on single bulk analyses of major elements by X-ray fluorescence (XRF) or inductively coupled plasma-optical emission spectrometry (ICP-OES).

Bioapatite in bone is chemically more complex than end-member hydroxylapatite, as well as typically defect-rich and non-stoichiometric. There are numerous chemical substitutions in bone apatite, the most important of which is the substitution of carbonate (McConnell, 1970; LeGeros,

1981; Rey et al., 1989; Daculsi et al., 1997; Peters et al., 2000; Elliott, 2002; Dorozhkin, 2007), and the degree of carbonation differs among vertebrate groups (Biltz and Pellegrino, 1969; Rey et al., 1989). It is the PO_4^{3-}, and to a lesser extent, the OH^- ions that undergo substitution by CO_3^{2-}. The charge imbalance is compensated by depleting calcium and hydroxyl ions in the mineral, thereby creating vacancies (LeGeros, 1981; Elliott, 2002; Rey et al., 2007b). Bone mineral's stoichiometry and composition are better represented by a formula such as $(Ca,Mg,Na)_{10-x}[(PO_4)_{6-x}(CO_3)_x](OH)_{2-x}$ (Elliott, 2002; Rey et al., 2007b), which reflects the interconnections among substitution, charge balance, and creation of vacancies. Despite the recognized fact that not all bone has an identical mineral composition, our understanding of bioapatite and our ability to test the appropriateness of formulae like the one above would be enhanced by the acquisition of better mineral analyses in selected bone samples.

A biological tissue bearing all the features of bone, yet extremely low in collagen, would be the ideal sample on which to pursue the chemistry of bioapatite. With a reported mineral content of ~96 wt%, the rostrum of the whale *Mesoplodon densirostris* is the densest bone recorded (de Buffrénil and Casinos, 1995; Zylberberg et al., 1998; Rogers and Zioupos, 1999) and an optimal choice for understanding the chemistry of bone mineral. Our previous studies by Raman spectroscopy, scanning electron microscopy, and histology confirmed that the rostrum truly is composed of bone (Li et al., 2013), rather than, for instance, a tissue more like the equally hypermineralized material of tooth enamel. Bone with such a high mineral content could be chemically analyzed much the way we analyze rocks, without the need to resort to often-used techniques for chemically stripping the collagen from the bone (Tomazic et al., 1993; Karampas et al., 2012). Therefore, unprocessed rostrum is an ideal material in which to investigate the inherent composition of bone mineral.

The goal of this study is to apply analytical techniques typically used on rocks and minerals, i.e., electron microprobe (EMP), XRF, thermogravimetric analysis (TGA), and carbon analysis to define the composition of bone mineral, using untreated rostrum. Both bulk chemistry and micrometer-scale variations in spot chemistry were studied within the whale rostrum.

MATERIALS AND METHODS

Sample Preparation

The rostrum sample investigated comes from a *M. densirostris* skeleton of a modern adult male (#1922-143) housed in the Muséum National d'Histoire Naturelle in Paris, France. The body length of *M. densirostris* ranges from 4.0 to 4.7 m in adult males, which are dark gray dorsally and ventrally. The histology, mechanical properties, and texture of other portions of this same rostrum have been reported earlier (de Buffrénil and Casinos, 1995; Rogers and Zioupos, 1999; Currey, 2003; Lambert et al., 2011; Li et al., 2013).

A rectangular prism of the rostrum material was cut using an Isomet low-speed, diamond-edged saw (Buehler LTD) to prepare the following two thin sections. 1) A longitudinal section (LE) was sawn and epoxied onto a glass plate. For subsequent optical microscopy and electron microprobe analyses, it was thinned to several tens of micrometers by careful grinding and polishing down to 1 μm diamond powder. 2) An additional longitudinal section (LC) was carefully polished down to 1 μm diamond powder while glued to a glass slide by cyanoacrylate (Superglue®, Loctite). The 1-mm thickness of this section allowed its surface to remain free of glue during grinding. It was studied by electron microprobe for comparison with the epoxied section.

In preparation for XRF analyses, an additional prism of the MNHN rostrum was heated in air at 650°C in an FB 1400 (Barnstead Thermolyne) furnace for 12 hours in order to volatilize organic components. For subsequent comparison, samples of lamb femur (from local butcher, 1.5-2 years old), elk antler (from local collector, less than one year old), and synthetic OHAP powder (Acros), were also ashed by the same procedure as the rostrum. This temperature and time have been shown sufficient to remove collagen from the bone (LeGeros and LeGeros, 1984; Mkukuma et al., 2004). The ashed materials were then analyzed by XRF.

Instrumentation

The polished sections underwent electron microprobe analysis using a JEOL JXA 8200 Superprobe in the Department of Earth and Planetary Sciences at Washington University in St. Louis (MO), operated with an accelerating voltage of 15 kV. Quantitative point analysis was accomplished with a beam current of 25 nA and a beam diameter 20 μm. Although finer spatial resolution is possible, the electron beam was kept broad to reduce damage to the nanocrystalline samples. The elements F, Na, Mg, P, S, Cl, K, Ca, and Sr were selected for quantitative analysis by wavelength-dispersive X-ray spectroscopy (WDS). The calibration standards for the EMP analyses included albite for Na analysis, Durango apatite for Ca, P, and F, synthetic forsterite for Mg, anhydrite for S, microcline for K, tugtupite for Cl, and Corning 95-IRX glass for Sr. In the creation of elemental maps, the element-specific X-rays generated by Ca, Cl, K, Na, and P were collected by an energy-dispersive spectrometer, and the elements F, S, and Mg were analyzed by a wavelength-dispersive spectrometer. For elemental mapping, the diameter of the electron beam was 3 μm and the analysis time for each pixel was 65 ms.

The bulk chemical compositions of the ashed rostrum, lamb femur, elk antler, and synthetic apatite (Acros) were analyzed by XRF, using a Siemens (now Bruker) SRS-300 X-ray spectrometer. The samples (~1 gram each) were ground to < 200 mesh, dried at 110 ^{o}C to remove adsorbed water and then ignited in a clean alumina ceramic crucible at 925 ^{o}C for XRF analysis. NIST-1486 bone meal (NIST, 2002) was also analyzed for calibration. The details of the sample preparation, data acquisition, and calibration of the XRF instrument have been reported previously (Couture et al., 1993) .

Samples of the rostrum and lamb femur were analyzed by using a TA Q500 thermogravimetric analyzer (TA Instruments) at Franklin and Marshall Collage, Lancaster, PA. The TGA analysis used a flow rate of 60 ml/min of nitrogen while the samples (30 mg) were heated to 800 ^{o}C at a rate of 10 ^{o}C/min.

Total carbon (TC) and inorganic carbon (TIC) were analyzed by a CM5015 CO_2 coulometer (UIC Inc.) at the University of Kansas, Manhattan, KS. TC was determined by combusting the rostrum sample in a tube furnace at 950 ^{o}C and then measuring the evolved CO_2 in a coulometric titration cell. TIC was determined by adding perchloric acid to the sample and then measuring the evolved CO_2 gas. The details of the sample preparation and data acquisition for the TC and IC have been reported (Engleman et al., 1985; Jackson and Roof, 1992; Hirmas et al., 2012). Organic carbon (TOC) was calculated by difference: TOC = TC-TIC.

RESULTS

Electron microprobe analysis

Figure 1 shows elemental maps and a back-scattered electron (BSE) image of the epoxied thin section (LE). Red shades grays in the BSE image indicate regions that contain relatively heavy elements and green shades indicate relatively light elements, e.g., collagen-rich areas. Therefore, organic-rich areas, i.e., curvilinear features (like collagen or blood vessels) and vascular holes, can be identified. These organic-rich features also are evident in the elemental maps, as regions depleted (green) in Ca, P, Na, and K. The dominant, i.e., typical, areas in the rostrum demonstrate a homogeneous distribution of mineral as recognized by the homogeneity in the shading for major elements (Ca and P) and minor elements (Na, K, and Cl). In contrast, the organic-rich areas in an elongated vessel and around the vascular hole (see VH and VE in Fig. 1) show enrichment (red) in F, S, and Mg, but depletion in Ca, P, Na, K, and Cl. It should be noted that K and Cl are usually extremely low in concentration in bone. The epoxy contains measurable F, as Fig. 1 shows elevated F in the larger vascular hole filled with epoxy.

Eight quantitative spot analyses were performed in the mineral-dominated typical areas of the rostrum. An additional four analyses were made within 300 μm of the large vascular hole in Fig. 1. Histologic stained sections of comparable areas of the rostrum (Li et al., 2013) show that collagenous tissue can extend on the order of 300 μm outward from vascular holes. Over-all chemical homogeneity of the typical areas is indicated by the quantitative analyses (Table 1) and is also demonstrated in Figure 1. All spots show high concentrations of calcium and phosphorus. The average Ca/P molar ratio of the 12 analyses is ~1.73 ± 0.05 (see Table 1), slightly higher than the 1.67 of stoichiometric OHAP [$Ca_{10}(PO_4)_6(OH)_2$].

The analyses made in typical mineral-rich areas (spots #1-8 in Table 1) have similar concentrations not only of the major but also of the minor elements S, F, and Mg. The chemical homogeneity within these typical areas is consistent with previous Raman spectroscopic studies

(Li et al., 2013). However, the last four analyses, acquired around the vascular holes, show enrichments in F, S, and Mg (Table 1) compared to the mineral-dominated typical areas, thereby showing heterogeneity in the concentration of these elements. In typical areas, MgO, SO_3, and F have average values of 0.81 wt%, 0.50 wt%, and 0.37 wt% compared to spots #9-12 around the vascular holes, which have average concentration of 0.98 wt%, 0.99 wt%, and 1.1 wt%, respectively (Table 1). In addition, relative to Mg, F and S are more concentrated around the vascular hole (see the contrast in Fig. 1).

Sodium concentration is homogeneous within the typical areas (Na_2O: 1.53±0.11 wt%), but slightly higher than that around the vascular holes (Na_2O: 1.10±0.09 wt%),). Despite its low absolute concentration, sodium is the most abundant element analyzed except for Ca and P. Carbon has a higher abundance, but it was not explicitly analyzed by EMP. Chlorine and potassium appear homogeneously distributed, but with extremely low concentrations throughout typical areas.

Figure 2 shows the compositional correlations in the LE section among the four minor elements Na, Mg, F, and S. There is a strong positive correlation between S, F, and Mg, i.e., enrichment of these elements in spots #8-12 around the vascular hole. In contrast, Na's concentration shows a strong inverse correlation with respect to Mg, F, and S, in that Na's concentration is homogeneous in typical areas but depleted around the vascular hole.

The quantitative spot analyses (Table 2) on the LC section affixed with cyanoacrylate show a stoichiometry similar to that of the epoxied LE section. The only exception is the detection in LE of fluorine that demonstrably is due to the epoxy: 0.37±0.13 wt% (spots #1-8 in Table 1 of the LE section) vs. 0.22±0.20 wt% (spots #1-4 in Table 2 of the LC section) in typical areas. The

Ca/P ratio in the LC section is 1.71±0.02, also close to 1.73±0.05 for the LE section in Table 1. Both the major (Ca and P) and minor (Na, Mg, S, Cl, and K) element concentrations show strong similarity between the two sections. Four analyses around the vascular hole in the LC section also have elevated F, Mg, and S, together with a lower Na content than in the typical areas. It therefore appears that the epoxy in the LE section did not affect the EMP results except for analyses made directly inside the pits and vascular holes, which are filled with F-bearing epoxy.

The <100 wt% sums in both the LC and LE sections are mainly attributed to organics (collagen) in the bone, and to carbonate, water, and hydroxyl in the apatite, which were not directly detected by EMP. The EMP analyses in the typical areas within the LC section have a slightly higher (~1%) sum of weight (wt%) than those in the LE epoxied section.

The calculation of apatite formulae based on these analyses can provide information important to the chemistry of bioapatite, e.g., evaluation of the cation substitutions for calcium and estimation of the amount of carbonate substitution. Our Raman analyses (Li et al., 2013) show that the strongly dominant mechanism of carbonate incorporation in the rostrum bioapatite, as in all analyzed bioapatites (at least 85-90% of the total carbonate in bone mineral: Elliott, 1994, 2002), is by substitution for phosphate. Assuming that all of the carbonate substitutes for phosphate in the apatite of the rostrum, the mineral formulae can be represented as $(Ca,Mg,Na)_{10-x}[(PO_4)_{6-x}(CO_3)_x](OH)_{2-x}$ (Elliott, 2002); the coefficients of CO_3^{2-} (x) and OH^- (2-x) in the formulae are obtained by solving the equation: (Ca+Mg+0.5Na)/P = (10-x)/(6-x) (for charge balance, one Na^+ is considered as 0.5 M^{2+}). Then, the wt% carbonate and the amount of substitution of Ca by Mg and Na can be assessed (see Table 3). Table 3 shows that the model-dependent degree of carbonation in apatite within the rostrum ranges from 5.4 to 8.4 wt%. With the reasonable assumption that Mg and Na cations are incorporated into the apatite component of

the bone, rather than derived from the collagen, the appropriate cation/phosphorus ratio for evaluation is (Ca+Mg+0.5Na)/P, whose value is shifted up to 1.76-1.84 (Table 3), well beyond the expected 1.67 of OHAP. Based on Table 3 and the equation above, the rostrum has the following average formula:

$$(Ca_{8.54}Mg_{0.25}Na_{0.38})[(PO_4)_{4.99}(CO_3)_{1.01}](OH)_{0.99} \quad (1)$$

If only the first four spots in the mineral-dominated typical areas in Table 3 are considered, the formula can be modified to:

$$(Ca_{8.61}Mg_{0.20}Na_{0.42})[(PO_4)_{5.02}(CO_3)_{0.98}](OH)_{1.02} \quad (2)$$

Formula (2) is similar to formula (1), except for less Mg and more Na. The estimated values of carbonate (CO_3^{2+} wt%), based solely on charge balance as described above, are also almost identical: 6.7 wt% in Formula (1) vs. 6.5 wt% in Formula (2). Note that these two calculated formulae also show about half the hydroxyl concentration that is in stoichiometric OHAP.

XRF analyses of ashed bone

Pursuing the chemistry of the mineral component of bone through analysis of ashed bone was the widely accepted approach in previous research on bone (Dallemagne and Richelle, 1973; LeGeros and LeGeros, 1984; Bigi et al., 1997; Skinner, 2005). Hence, it is valuable to repeat this approach on the rostrum for comparison. Table 4 shows that the ashed rostrum has a slightly higher Ca/P ratio than those in more normal bone materials, like the lamb femur and elk antler of the present study. The ratio in the rostrum is also greater than that previously reported in human bone (ratio=1.65), as well as in human tooth enamel (ratio=1.58) (LeGeros and LeGeros, 1984; Daculsi et al., 1997). Ca/P ratios elevated above 1.67 are typically related to substitution of

carbonate for phosphate ($Ca_{10-x}/(PO_4)_{6-x}$) or to an increase in Ca during aging of bone (Legros et al., 1987; Skedros et al., 1993; Dorozhkin, 2007).

The Acros synthetic apatite and NIST-1486 bone meal show Ca/P ratios between those of the rostrum and those of normal bones. Their values lie within 0.01 units of the theoretical value of 1.67. The XRF-derived formula for rostrum bioapatite based on the same model as in Formulas (1) and (2) is:

$$(Ca_{8.40}Mg_{0.20}Na_{0.54})[(PO_4)_{4.87}(CO_3)_{1.13}](OH)_{0.87} \quad (3)$$

The calculated CO_3^{2-} concentration of the rostrum, based on charge-balancing of the XRF data, is 7.6 wt% (in the expected 6-8 wt% range for bone) based on formula (3). This value is slightly higher than the 6.7 wt% derived from formula (1) and based on EMP data. The value is also higher than the 3.5 wt% for human enamel (LeGeros and LeGeros, 1984) and the 6 wt% determined for a specific human bone (Daculsi et al., 1997) by bulk analyses of ashed materials.

Compared to the lamb femur and elk antler, the rostrum has 60 wt% more Na, but 40 wt% less Mg, although both minor elements are even less than one-twentieth of the weight of the major element Ca in all studied samples (see Table 4). The Mg concentration in the rostrum is similar to that in the synthetic OHAP and to the comparably hypermineralized (also ~95 wt% mineral) tooth enamel (LeGeros and LeGeros, 1984). However, concentrations of Na_2O in the Acros synthetic apatite (0.08 wt%) and in the tooth enamel (0.40 wt%) (LeGeros and LeGeros, 1984) are lower than in the rostrum. Trace elements Al, Si, Ti, and Fe, are extremely low in all bones and synthetic apatites as shown in Table 4.

Thermogravimetric analysis and carbon analysis

TGA was applied to investigate weight loss due to release of water (in collagen and structurally incorporated in apatite), breakdown of collagen, and breakdown of carbonate (within the apatite structure) for the unprocessed rostrum and lamb femur. Fig. 3 shows that the heated lamb femur has several weight loss stages (25 ^{o}C to 100 ^{o}C, 100 ^{o}C to 250 ^{o}C, 250 ^{o}C to 450 ^{o}C, 450 ^{o}C to 550 ^{o}C , 550 ^{o}C to 800 ^{o}C), which are not easily identified in the rostrum. The weight loss below 100 ^{o}C is typically ascribed to adsorbed water (Ivanova et al., 2001; Mkukuma et al., 2004; Yoder et al., 2012). The 7.1 wt% weight loss of the lamb femur below 100C ^{o} is larger than the 2.3 wt% loss of the rostrum, which probably is due to the presence of water in the abundant collagen fibers of the femur.

Weight loss in the lamb femur and the rostrum between 100 ^{o}C and 800 ^{o}C represents the breakdown of organics (e.g., collagen) and their release as volatiles, the decomposition of structurally incorporated carbonate and its release as CO_2, and the release of apatite's lattice water. The two TGA traces show a similar slope between 150 ^{o}C and 250 ^{o}C, which suggests the initial rates of breakdown of collagen within and release of water from collagen fibers are similar in the rostrum and lamb femur. Release of lattice water was reported to extend up to 550 ^{o}C in bone and synthetic carbonated apatite (LeGeros et al., 1978; Ivanova et al., 2001; Mason et al., 2009; Yoder et al., 2012). Organics are considered ashed by 600 ^{o}C (Mkukuma et al., 2004), but some carbonaceous residues may be stable to higher temperature (based on our Raman spectroscopy on heated samples). The breakdown of carbonate, released as CO_2 from apatite, can start as low as 350 ^{o}C (Ivanova et al., 2001). Therefore, it is impossible to recognize the isolated loss stages of organics, lattice water, and carbonate from Fig. 3. The rostrum has a cumulative 9.3 wt% loss by 550 ^{o}C, showing an almost linear release pattern. Further release occurs more

slowly up to 10.4 wt% by 800 °C. In contrast, the lamb femur loses an additional ~3 wt% from 550 °C to 800 °C, which is probably due to further breakdown of abundant organic residue.

Coulometric analysis of unprocessed rostrum yields TIC of 1.57±0.04 wt%. The calculated amount of carbonate (CO_3^{2-}) is 7.88±0.22 wt% (Table 5), which is within the range of bone apatite's carbonate in Table 3 as calculated from EMP analyses. Furthermore, it approaches the 7.6 wt% carbonate in formula (3) derived from XRF analysis. Raman calibration on a suite of synthetic carbonated apatites analyzed in our group (Pasteris et al., 2008) permitted the spectroscopic evaluation of the carbonate concentration in bioapatite. The carbonate values in the rostrum bone apatite average 7.96±0.35 wt% (N=10), also close to the value of the present carbon analysis. Our three independent means of directly or indirectly determining carbonate in bioapatite are therefore in good agreement.

As seen in Table 5, the breakdown of all CO_3^{2-} leads to a 5.76 wt% loss due to evolved CO_2. Consider this weight loss in the context of Fig. 3, which shows a total loss of 10.4 wt% up to 800 °C, representing losses of water, collagen, and carbonate. The difference between the total weight loss and the weight loss due to carbonate breakdown (10.4 - 5.7 wt%) can be attributed to loss of water and collagen (4.6 wt%; see equation 4).

Carbonate Loss = Total Loss – (Water Loss + Collagen Loss) (up to 800 °C) (4)

The inferred mineral content of the rostrum is 95.4 wt% (100 wt% - 4.6 wt%), which matches the ~95-96 wt% mineral content reported in the literature (de Buffrénil and Casinos, 1995; Zylberberg et al., 1998; Rogers and Zioupos, 1999) and based on our previous Raman analysis (Li et al., 2013). The TOC equals TC - TIC, i.e., 0.91±0.04 wt%, which is primarily from collagen.

DISCUSSION

The only recognized mineral in the rostrum, as in all normal bones, is carbonated OHAP. The stoichiometry of the bioapatite in the rostrum is shown to match that of bone and to differ significantly from that of the similarly hypermineralized material, enamel. The mineral in the rostrum has a Ca/P atomic ratio ranging from 1.68 to 1.82 based on EMP point analyses, which are in good agreement with the ratio of 1.73 based on XRF bulk analyses. These values are slightly higher than the 1.67 of synthetic OHAP and the ~1.65 of two common bones (lamb femur and elk antler). Increased amounts of substitution of carbonate for phosphate in the rostrum compared to that in some other bones could cause such a shift in Ca/P atomic ratios.

Previous data on the chemistry of bone and bone mineral are scarce, e.g., in the absence of new data, the same analysis of human bone (LeGeros, 1981; LeGeros and LeGeros, 1984) has been cited in many recent articles. Furthermore, the data are problematic: 1) Some inconsistencies or typographical errors exist in the published tables, e.g., P is listed as 10.5 wt% in LeGeros 1981 vs. 11.5 wt% in LeGeros and LeGeros 1984; 2) These data are shown to only one decimal place, making the calculation of carbonate and hydroxyl concentrations impossible. The present EMP and XRF analyses of the rostrum therefore elucidate the most accurate chemistry known for the unprocessed bone. Calculated formulas based on the model of $(Ca,Mg,Na)_{10-x}[(PO_4)_{6-x}(CO_3)_x](OH)_{2-x}$ (Elliott, 2002) show the relative ion concentrations of the bioapatite in the rostrum (Table 6). Formulae (1) and (2) based on EMP analyses are valuable in tracking chemical variation within the rostrum. Formula (3) based on XRF bulk analysis provides the closest estimation of the average stoichiometry of the bioapatite in the rostrum.

Both EMP and XRF analyses show that Na is the third most abundant element (excluding oxygen) in the rostrum bioapatite, following the major elements Ca and P. The substitution of carbonate for phosphate is known to be coupled with that of Na for Ca in bioapatites (LeGeros, 1981; Elliott, 1994; Daculsi et al., 1997; Cazalbou et al., 2004; Peroos et al., 2006; Barinov et al., 2008), which leads to co-incorporation of carbonate and sodium in bone. This complex substitution mechanism is well illustrated by the rostrum. All bones have a markedly higher Na concentration than does usual synthetic OHAP that is not carbonated (see Table 4). The concentration of Na in the rostrum is also higher than that in typically analyzed human bones and tooth enamel (LeGeros and LeGeros, 1984; Daculsi et al., 1997) and in the ashed lamb femur and elk antler analyzed here. The hypermineralized areas of the rostrum have higher sodium concentrations than the organic-rich areas, which further supports the notion of the crystallographic incorporation of bone's Na component within the mineral.

Elevation in the concentration of S, F, and Mg around the organic-enriched vascular holes suggests that the organic matter contains these elements. However, these ions are present in both the organic and inorganic components of bone, as the highly mineralized typical areas also show considerable concentration of those elements. In apatite, SO_4^{2-} can substitute for PO_4^{3-}, much like CO_3^{2-} does (Glimcher, 1959; Legros et al., 1987; Elliott, 1994; 1997; Glimcher, 2006). Fluoride incorporation is prevalent although typically low in concentration in bioapatite, in which fluoride ions share channel sites with hydroxyl ions (LeGeros and LeGeros, 1984; Elliott, 1994; Elliott, 2002; Dorozhkin, 2007; Kuhn et al., 2008; Dorozhkin, 2009; Pasteris and Ding, 2009). Substitution of Mg cations for Ca in bioapatite also has been widely reported (LeGeros, 1981; LeGeros and LeGeros, 1984; Elliott, 1994; Tampieri et al., 2005). Mg incorporation may reduce the crystallinity and the solubility of apatite (LeGeros and LeGeros, 1984; LeGeros et al., 1995).

The higher degree (compared to normal bones) of mineral crystallinity in the rostrum based on Raman spectroscopy (Li et al., 2013) and X-ray diffraction (Rogers and Zioupos, 1999), compared to normal bones, could be due in part to the rostrum's lower Mg concentration (see Table 4). Sulfur can be incorporated in apatite as SO_4 (substituting for PO_4), whereas fluoride can substitute for OH. Tellingly, the SO_4^{2-} and F^- in rostrum apatite are even more strongly correlated with the presence of organic matter than Mg is (see contrast of elemental maps in Fig. 1). In Table 2, the average concentrations of F and SO_3 in typical areas are only ~19% and ~38%, respectively, of those in areas around the vascular hole. For MgO, in comparison, the value is ~63%. These data suggest that Mg is partitioned more strongly into the mineral than F^- and SO_4^{2-}. It is therefore reasonable to represent the stoichiometry of the mineral phase in the rostrum as $(Ca,Mg,Na)_{10-x}[(PO_4)_{6-x}(CO_3)_x](OH)_{2-x}$ (Elliott, 2002), which excludes S and F.

Chlorine and potassium are distributed homogeneously in the typical areas of the rostrum, but at an extremely low concentration (~1/1000 of the calcium). Due to the ion's relatively large size, to incorporate appreciable Cl into apatite formed in a low-temperature aqueous environment requires a very high Cl concentration in the coexisting solution (LeGeros, 1975). The low concentration of K in bioapatite is likewise due to its large radius (Elliott, 1994) and low concentration in body fluid. Other trace elements, e.g., Al, Fe, Si, Ti, and Sr, are all near or below the detection limits of the XRF and EMP analyses made in this study.

Carbon analysis shows that the rostrum has ~8 wt% carbonate, assumed to be entirely in the bioapatite. This carbonate content is at the high end (but not the highest value (Li et al., 2013)) of the bone materials studied in our lab, and within the 6-8 wt% carbonate range typically cited in the literature (LeGeros and LeGeros, 1984; Elliott, 2002; Glimcher, 2006). The ~8 wt% value is consistent with our calculated value of 7.6 wt% based on the compositional model of

$(Ca,Mg,Na)_{10-x}[(PO_4)_{6-x}(CO_3)_x](OH)_{2-x}$. Therefore, this model is valuable in estimating unanalyzed components in a formula for bone apatite. In addition to carbonate estimation, the model provides a plausible method by which to estimate hydroxyl, which is difficult to assess by most techniques.

The rostrum bioapatite has less than half the hydroxyl molar content of OHAP (see Table 6). In an equilibrium system of CaO-PO_4-CO_2-H_2O, as carbonate substitution increases in the apatite, the OH-concentration decreases (Pasteris et al., 2012). However, the presence of Na^+ as a substitute for Ca^{2+} provides an alternative to the basic mechanism of $(PO_4)^{3-} + Ca^{2+} + OH^- \leftrightarrow (CO_3)^{2-} + \square_{Ca} + \square_{OH}$, in which the addition of each mole of $(CO_3)^{2-}$ produces one mole of OH-vacancies. In contrast, the availability of Na^+ permits substitution of $(PO_4)^{3-} + Ca^{2+} \leftrightarrow (CO_3)^{2-} + Na^+$, which does not demand any vacancies in the OH-site. Therefore, although the concentration of carbonate in the rostrum is at the high end of that typically reported in bone mineral, the degree of hydroxyl depletion is not as great in the rostrum as in some other reported bone analyses (LeGeros and LeGeros, 1984; Legros et al., 1987; Daculsi et al., 1997; Cho et al., 2003; Kolmas and Kolodziejski, 2007).

A deficiency in the wt% totals was displayed in all the quantitative EMP spot analyses (Table 1 and 2) of the rostrum. Since the light elements carbon, hydrogen, and nitrogen, and other minor elements were not analyzed for, the sum of the weights, as detected in each spot should be less than ~90 percent. For example, CO_2 within the rostrum is 5.76 wt% (see Table 5), and H_2O contributes 1.1 wt% (converted from OH in formula 3). Low-temperature, aqueously precipitated carbonated OHAP, including bioapatites, also contain about 3 wt% structurally incorporated water (Yoder et al., 2012). Considering an additional ~4 wt% of organic matter in the rostrum (Li et al., 2013), would produce a total expected deficit of ~14 wt%.

All of the formulas presented above are model-dependent, as explained in the analytical sections. They follow accepted protocols, however, which permit comparison of our analyses with those of other types of bioapatite (e.g., tooth enamel) and with future analyses of bone mineral. One other assumption in our data presentation, as in that of all other chemical analyses of bioapatite known to us, is that the elements analyzed are crystallographically incorporated in the mineral structure. It is well known that carbonated apatite including that in bone has a highly reactive surface (also a high surface-area-to-volume ratio) with a high concentration of adsorbed ions (Cazalbou et al., 2004; Rey et al., 2007a; Rey et al., 2007b). The adsorbed species, however, are difficult to quantify and have not been addressed in the current work.

Agreement between EMP on raw rostrum and XRF on ashed rostrum supports our contention that the rostrum provides an ideal example of bone mineral, which can be chemically analyzed without resorting to processing techniques that can alter the bone mineral. In-situ EMP analysis is preferable in order to track chemical variation within the rostrum. The XRF is more precise in evaluating the chemistry of the bulk material, e.g., the estimated carbonate concentration based on XRF-derived formula (3) approaches the independent carbon analysis more closely than do the EMP analyses.

CONCLUDING REMARKS

The rostrum does not require complicated and chemically intense processes of sample preparation, e.g., deproteinization (thereby avoiding the mineral dissolution/re-precipitation during chemical stripping of organics) or ashing (thereby avoiding contamination of the bone mineral by residual non-volatile ions from the collagen). For EMP, the rostrum permits in-situ point analysis and elemental mapping on the fresh sample. For XRF bulk analysis on ashed

material, the rostrum produces extremely low concentrations of ion residues from collagen. Good correlation between EMP point analyses and XRF bulk analyses of ashed rostrum show the latter to be a useful chemical model of bone mineral. This finding is important, because it demonstrates that the rostrum can be analyzed without removal of collagen by heating/ashing or chemical stripping, which can chemically compromise the mineral component of normal bone.

The carbonated hydroxylapatite in the rostrum has ~8 wt% carbonate and an elevated Ca/P ratio of 1.7 as measured directly by EMP. The Mg concentration in the analyzed materials shows the order: normal bones>rostrum ≈ enamel>synthetic OHAP, whereas for Na the order is rostrum>normal bones>enamel>synthetic OHAP. The rostrum has extremely low trace element concentrations, e.g., Cl, K, Al, Si, Fe, and Ti. Slightly higher S, F, and Mg concentrations around vascular holes could be related to enrichment in organics, but most Mg resides in the mineral. Both Na and Mg appear to be incorporated into the Ca sites in the bioapatite.

The chemistry of bioapatite varies among different vertebrates and different bones of the same vertebrate, producing variations in both the bulk mineral composition and exact stoichiometry of the bioapatite analyzed (Biltz and Pellegrino, 1977). In addition, some of the analyzed ions might be adsorbed on the surface of the mineral rather than incorporated in the crystal structure. However, as a hypermineralized bone with 95-96 wt% mineral content, the rostrum is still an ideal material in which to investigate the chemistry of bioapatite, and therefore is an excellent exemplar of "bone mineral." The present multiple analyses of bone mineral contribute to the scant published literature currently available.

ACKNOWLEDGEMENTS

The work is partially funded by NIH grant 1R21AR055184-01A2. We thank Dr. Vivian de Buffrénil and Dr. Olivier Lambert for the MNHN rostrum sample. We thank Dr. Rex Couture and Prof. Robert Dymek for the XRF analyses and Paul Carpenter for assistance with EMP analyses. We also thank Prof. Daniel Hirmas for the carbon analyses and Prof. Claude Yoder for the thermogravimetric analyses.

REFERENCES CITED

Barinov, S.M., Fadeeva, I.V., Ferro, D., Rau, J.V., Cesaro, S.N., Komlev, V.S., and Fomin, A.S. (2008) Stabilization of carbonate hydroxyapatite by isomorphic substitutions of sodium for calcium. Russian Journal of Inorganic Chemistry, 53, 164-168.

Bigi, A., Cojazzi, G., Panzavolta, S., Ripamonti, A., Roveri, N., Romanello, M., Suarez, K.N., and Moro, L. (1997) Chemical and structural characterization of the mineral phase from cortical and trabecular bone. Journal of Inorganic Biochemistry, 68, 45-51.

Biltz, R.M., and Pellegrino, E.D. (1969) The chemical anatomy of bone. I. A comparative study of bone composition in sixteen vertebrates. The Journal of Bone and Joint Surgery, 51, 456-466.

-. (1977) The nature of bone carbonate. Clinical Orthopaedics and Related Research, 129, 279-292.

Biltz, R.M., Pellegrino, E.D., and Letteri, J.M. (1981) Skeletal carbonates and acid-base regulation. Mineral and Electrolyte Metabolism, 5, 1-7.

Cazalbou, S., Combes, C., Eichert, D., and Rey, C. (2004) Adaptative physico-chemistry of bio-related calcium phosphates. Journal of Materials Chemistry, 14, 2148-2153.

Cho, G.Y., Wu, Y.T., and Ackerman, J.L. (2003) Detection of hydroxyl ions in bone mineral by solid-state NMR spectroscopy. Science, 300, 1123-1127.

Couture, R.A., Smith, M.S., and Dymek, R.F. (1993) X-ray-fluorescence analysis of silicate rocks using fused glass disks and a side-window Rh source tube - accuracy, precision and reproducibility. Chemical Geology, 110, 315-328.

Currey, J.D. (1979) Mechanical properties of bone tissues with greatly differing functions. Journal of Biomechanics, 12, 313-319.

-. (2002) Bones: structure and mechanics. In J.D. Currey, Ed. The structure of bone tissue, p. 12-20. Princeton University Press, Princeton.

-. (2003) Role of collagen and other organics in the mechanical properties of bone. Osteoporosis International, 14 Suppl 5, S29-S36.

Daculsi, G., Bouler, J.M., and LeGeros, R.Z. (1997) Adaptive crystal formation in normal and pathological calcifications in synthetic calcium phosphate and related biomaterials. International Review of Cytology, 172, 129-189.

Dallemagne, M.J., and Richelle, L.J. (1973) Inorganic chemistry of bone. In I. Zipkin, Ed. Biological Mineralization, p. 23-42 John Wiley, New York.

de Buffrénil, V., and Casinos, A. (1995) Observations histologiques sur le rostre de Mesoplodon densirostris (Mammalia, Cetacea, Ziphiidae): le tissu osseux le plus dense connu. Zoologie et Biologie Animale, 16, 21-32.

Dorozhkin, S.V. (2007) Calcium orthophosphates. Journal of Materials Science, 42, 1061-1095.

-. (2009) Calcium orthophosphate-based biocomposites and hybrid biomaterials. Journal of Materials Science, 44, 2343-2387.

Driessens, F.C. (1982) Mineral aspects of dentistry. Monographs in Oral Science, 10, 1-215.

Elliott, J.C. (1994) Fluorapatite and chlorapatite. In J.C. Elliott, Ed. Structure and Chemistry of the Apatites and Other Calcium Orthophosphates p. 63-104. Elsevier, The Netherlands.

-. (2002) Calcium phosphate biominerals. In M.J. Kohn, J. Rakovan, and J.M. Hughes, Eds. Phosphates: Geochemical, Geobiological, and Materials Importance, 48, p. 427-453. Reviews in Mineralogy and Geochemistry, Mineralogical Society of America, Chantilly, Virginia.

Engleman, E.E., Jackson, L.L., and Norton, D.R. (1985) Determination of carbonate carbon in geological-materials by coulometric titration. Chemical Geology, 53, 125-128.

Glimcher, M.J. (1959) Molecular biology of mineralized tissues with particular reference to bone. Reviews of Modern Physics, 31, 359-393.

-. (2006) Bone: nature of the calcium phosphate crystals and cellular, structural, and physical chemical mechanisms in their formation. In N. Sahai, and M.A.A. Schoonen, Eds. Medical Mineralogy and Geochemistry, 64, p. 223-282. Reviews in Mineralogy and Geochemistry, Mineralogical Society of America, Washington, D.C.

Hirmas, D.R., Platt, B.F., and Hasiotis, S.T. (2012) Determination of calcite and dolomite content in soils and paleosols by continuous coulometric titration. Soil Science Society of America Journal, 76, 1100-1106.

Ivanova, T.I., Frank-Kamenetskaya, O.V., Kol'tsov, A.B., and Ugolkov, V.L. (2001) Crystal structure of calcium-deficient carbonated hydroxyapatite. Thermal decomposition. Journal of Solid State Chemistry, 160, 340-349.

Jackson, L.L., and Roof, S.R. (1992) Determination of the forms of carbon in geologic materials. Geostandards Newsletter, 16, 317-323.

Karampas, I.A., Orkoula, M.G., and Kontoyannis, C.G. (2012) Effect of hydrazine based deproteination protocol on bone mineral crystal structure. Journal of Materials Science--Materials in Medicine, 23, 1139-1148.

Kolmas, J., and Kolodziejski, W. (2007) Concentration of hydroxyl groups in dental apatites: a solid-state H^1 MAS NMR study using inverse P^{31} -> H^1 cross-polarization. Chemical Communications, 4390-4392.

Kuhn, L.T., Grynpas, M.D., Rey, C.C., Wu, Y., Ackerman, J.L., and Glimcher, M.J. (2008) A comparison of the physical and chemical differences between cancellous and cortical bovine bone mineral at two ages. Calcified Tissue International, 83, 146-154.

Lambert, O., de Buffrénil, V., and de Muizon, C. (2011) Rostral densification in beaked whales: diverse processes for a similar pattern. Comptes Rendus Palevol, 10, 453-468.

LeGeros, R.Z. (1975) The unit cell dimensions of human enamel apatite. Archives of Oral Biology, 20, 63-71.

-. (1981) Apatites in biological-systems. Progress in Crystal Growth and Characterization of Materials, 4, 1-45.

LeGeros, R.Z., Bonel, G., and Legros, R. (1978) Types of "H_2O" in human enamel and in precipitated apatites. Calcified Tissue International, 26, 111-118.

LeGeros, R.Z., Kijkowska, R., Bautista, C., and LeGeros, J.P. (1995) Synergistic effects of magnesium and carbonate on properties of biological and synthetic apatites. Connective Tissue Research, 32, 525-531.

LeGeros, R.Z., and LeGeros, J. (1984) Phosphate minerals in human tissues. In J.O. Nriagu, and P.B. Moore, Eds. Phosphate Minerals, p. 351-384. Springer, New York.

LeGeros, R.Z., Trautz, O.R., Klein, E., and LeGeros, J.P. (1969) Two types of carbonate substitution in the apatite structure. Experientia, 25, 5-7.

Legros, R., Balmain, N., and Bonel, G. (1987) Age-related changes in mineral of rat and bovine cortical bone. Calcified Tissue International, 41, 137-144.

Li, Z., Pasteris, J.D., and Novack, D. (2013) Hypermineralized whale rostrum as the exemplar for bone mineral. Connective Tissue Research, 54, 167-175.

Mason, H.E., McCubbin, F.M., Smirnov, A., and Phillips, B.L. (2009) Solid-state NMR and IR spectroscopic investigation of the role of structural water and F in carbonate-rich fluorapatite. American Mineralogist, 94, 507-516.

McConnell, D. (1962) The crystal structure of bone. Clinical Orthopaedics and Related Research, 23, 253-268.

-. (1970) Crystal chemistry of bone mineral - hydrated carbonate apatites. American Mineralogist, 55, 1659-1669.

Mitchell, L., Faust, G.T., Hendricks, S.B., and Reynolds, D.S. (1943) The mineralogy and genesis of hydroxylapatite. American Mineralogist, 28, 356-377.

Mkukuma, L.D., Skakle, J.M., Gibson, I.R., Imrie, C.T., Aspden, R.M., and Hukins, D.W. (2004) Effect of the proportion of organic material in bone on thermal decomposition of bone mineral: an investigation of a variety of bones from different species using thermogravimetric analysis coupled to mass spectrometry, high-temperature X-ray diffraction, and Fourier transform infrared spectroscopy. Calcified Tissue International, 75, 321-328.

NIST. (2002) SRM 1486 - bone meal. https://www-s.nist.gov/srmors/view_detail.cfm?srm=1486.

Pan, Y.M., and Fleet, M.E. (2002) Compositions of the apatite-group minerals: substitution mechanisms and controlling factors. In M.J. Kohn, J. Rakovan, and J.M. Hughes, Eds. Phosphates: Geochemical, Geobiological, and Materials Importance, 48, p. 13-49. Reviews in Mineralogy and Geochemistry, Mineralogical Society of America, Chantilly, Virginia.

Pasteris, J.D., and Ding, D.Y. (2009) Experimental fluoridation of nanocrystalline apatite. American Mineralogist, 94, 53-63.

Pasteris, J.D., Wopenka, B., and Man, S. (2008) Concerning the cause of the 1070 Δcm^{-1} Raman band in carbonated apatite. Abstract for 8th Biomaterials Congress, p. A478.

Pasteris, J.D., Yoder, C.H., Sternlieb, M.P., and Liu, S. (2012) Effect of carbonate incorporation on the hydroxyl content of hydroxylapatite. Mineralogical Magazine, 76, 2741-2759.

Peroos, S., Du, Z.M., and de Leeuw, N.H. (2006) A computer modelling study of the uptake, structure and distribution of carbonate defects in hydroxy-apatite. Biomaterials, 27, 2150-2161.

Peters, F., Schwarz, K., and Epple, M. (2000) The structure of bone studied with synchrotron X-ray diffraction, X-ray absorption spectroscopy and thermal analysis. Thermochimica Acta, 361, 131-138.

Rey, C., Collins, B., Goehl, T., Dickson, I.R., and Glimcher, M.J. (1989) The carbonate environment in bone mineral -- a resolution-enhanced Fourier transform infrared spectroscopy study. Calcified Tissue International, 45, 157-164.

Rey, C., Combes, C., Drouet, C., Lebugle, A., Sfihi, H., and Barroug, A. (2007a) Nanocrystalline apatites in biological systems: characterisation, structure and properties. Materialwissenschaft und Werkstofftechnik, 38, 996-1002.

Rey, C., Combes, C., Drouet, C., Sfihi, H., and Barroug, A. (2007b) Physico-chemical properties of nanocrystalline apatites: implications for biominerals and biomaterials. Materials Science & Engineering C--Biomimetic and Supramolecular Systems, 27, 198-205.

Rogers, K.D., and Zioupos, P. (1999) The bone tissue of the rostrum of a Mesoplodon densirostris whale: a mammalian biomineral demonstrating extreme texture. Journal of Materials Science Letters, 18, 651-654.

Skedros, J.G., Bloebaum, R.D., Bachus, K.N., Boyce, T.M., and Constantz, B. (1993) Influence of mineral-content and composition on graylevels in backscattered electron images of bone. Journal of Biomedical Materials Research, 27, 57-64.

Skinner, H.C.W. (2005) The web of magnesium. International Geology Review, 47, 1111-1119.
Tampieri, A., Celotti, G., and Landi, E. (2005) From biomimetic apatites to biologically inspired composites. Analytical and Bioanalytical Chemistry, 381, 568-576.
Tomazic, B.B., Brown, W.E., and Eanes, E.D. (1993) A critical-evaluation of the purification of biominerals by hypochlorite treatment. Journal of Biomedical Materials Research, 27, 217-225.
Yoder, C.H., Pasteris, J.D., Worcester, K.N., and Schermerhorn, D.V. (2012) Structural water in carbonated hydroxylapatite and fluorapatite: confirmation by solid state H^2 NMR. Calcified Tissue International, 90, 60-67.
Zioupos, P., Currey, J.D., and Casinos, A. (2000) Exploring the effects of hypermineralisation in bone tissue by using an extreme biological example. Connective Tissue Research, 41, 229-248.
Zylberberg, L., Traub, W., De Buffrenil, V., Allizard, F., Arad, T., and Weiner, S. (1998) Rostrum of a toothed whale: ultrastructural study of a very dense bone. Bone, 23, 241-247.

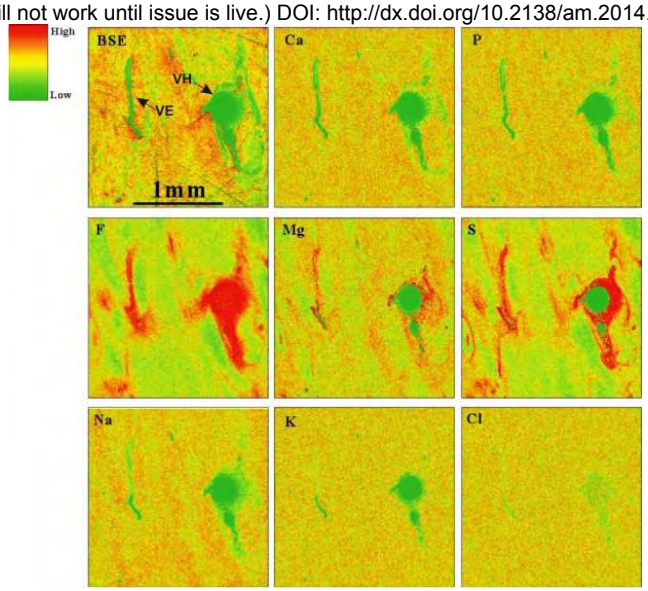

FIGURE 1. Back-scattered electron image and elemental maps of a 1.95×1.95 mm area in the epoxied LE section. The section shows a round vascular hole (VH) and an elongated vessel (VE) in addition to mineral-dominated bone.

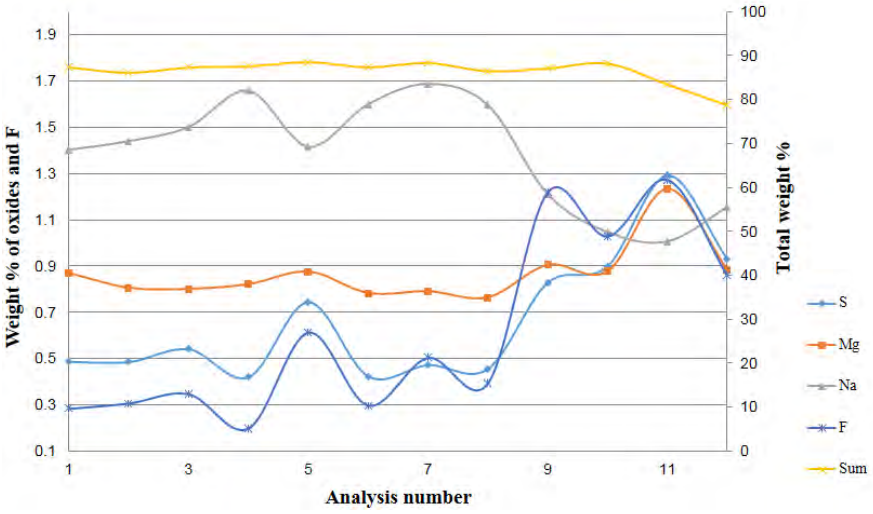

FIGURE 2. Variations of S, F, Mg, and Na (S, Mg, and Na are shown as oxides) and total wt% of analyses in the LE section. See Table 1 for original data and uncertainties.

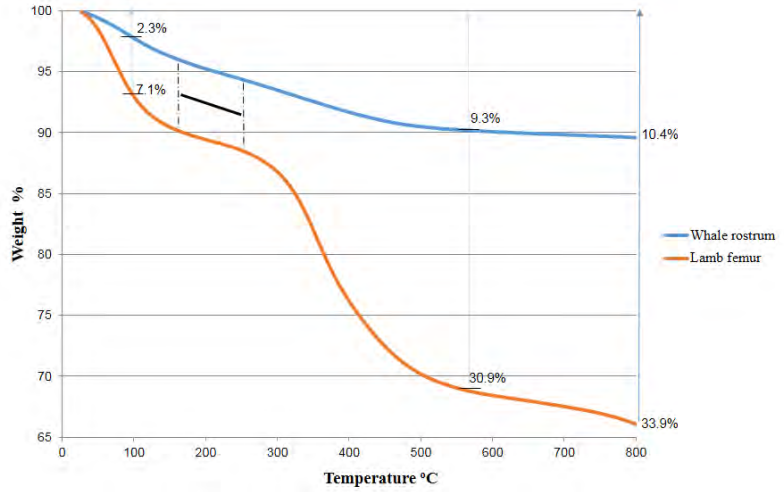

FIGURE 3. TGA traces of the whale rostrum and lamb femur.

TABLE 1. EMP quantitative analyses in typical areas and near vascular holes (⬥) in the LE section affixed with epoxy. The sum of the analyzed weight percents is also included. Analyses #9-12 were taken within 300 μm of the vascular hole in Fig. 1. All values shown are in wt% except for the Ca/P atomic ratios.

#	CaO	P_2O_5	Na_2O	MgO	SO_3	K_2O	Cl	F	SrO	Ca/P	Sum
1	48.60 (0.6)	35.58 (0.5)	1.40 (2)	0.87 (2)	0.49 (2)	0.03 (12)	0.04 (7)	0.28 (6)	-	1.73	87.29
2	47.65 (0.6)	35.30 (0.5)	1.44 (1)	0.81 (2)	0.48 (2)	0.02 (17)	0.04 (8)	0.31 (5)	0.03 (45)	1.71	86.08
3	48.17 (0.6)	35.82 (0.5)	1.50 (1)	0.80 (2)	0.54 (2)	0.02 (14)	0.04 (7)	0.35 (5)	0.03 (50)	1.70	87.27
4	48.65 (0.6)	35.66 (0.5)	1.66 (1)	0.82 (2)	0.42 (3)	0.04 (10)	0.04 (8)	0.20 (8)	0.06 (26)	1.73	87.55
5	48.57 (0.6)	36.16 (0.5)	1.41 (1)	0.88 (2)	0.74 (2)	0.03 (11)	0.05 (6)	0.61 (3)	0.03 (47)	1.70	88.48
6	48.73 (0.6)	35.39 (0.5)	1.60 (1)	0.78 (2)	0.42 (3)	0.03 (10)	0.04 (8)	0.30 (5)	0.03 (58)	1.74	87.32
7	48.50 (0.6)	36.24 (0.5)	1.69 (1)	0.79 (2)	0.47 (3)	0.03 (10)	0.03 (10)	0.50 (3)	0.03 (59)	1.69	88.28
8	48.12 (0.6)	35.03 (0.5)	1.59 (1)	0.76 (2)	0.46 (3)	0.03 (11)	0.04 (8)	0.39 (4)	0.02 (67)	1.74	86.44
9⬥	47.24 (0.6)	35.54 (0.5)	1.21 (2)	0.90 (1)	0.83 (2)	0.03 (13)	0.04 (8)	1.22 (1)	0.05 (27)	1.68	87.06
10⬥	48.96 (0.6)	35.24 (0.5)	1.05 (2)	0.88 (2)	0.90 (2)	0.02 (17)	0.02 (13)	1.03 (2)	0.05 (30)	1.76	88.15
11⬥	44.92 (0.6)	33.57 (0.5)	1.00 (2)	1.24 (1)	1.29 (3)	0.03 (13)	0.06 (6)	1.27 (1)	0.06 (26)	1.69	83.44
12⬥	43.76 (0.6)	31.09 (0.5)	1.15 (2)	0.88 (1)	0.93 (2)	0.02 (14)	0.04 (7)	0.86 (2)	0.04 (42)	1.78	78.77

"-": below detection limit. Parentheses: relative errors %.

TABLE 2. EMP quantitative analyses in typical areas and near vascular holes (◆) in the LC section affixed with cyanoacrylate. Analyses #5-8 were taken within 300 μm of the vascular holes. All values shown are in wt% except for the Ca/P atomic ratios.

#	CaO	P_2O_5	Na_2O	MgO	SO_3	K_2O	Cl	F	SrO	Ca/P	Sum
1	49.02 (0.1)	36.56 (0.2)	1.07 (1)	0.88 (3)	0.15 (6)	0.31 (2)	0.06 (9)	-	-	1.70	88.05
2	49.28 (0.2)	37.00 (0.4)	1.19 (2)	0.82 (2)	0.48 (3)	0.02 (22)	0.04 (10)	0.37 (6)	-	1.69	89.20
3	47.80 (0.2)	35.13 (0.5)	1.56 (2)	0.79 (2)	0.36 (3)	0.03 (16)	0.04 (9)	0.09 (23)	-	1.72	85.80
4	49.94 (0.2)	36.01 (0.5)	1.62 (2)	0.76 (2)	0.41 (3)	0.03 (21)	0.03 (11)	0.40 (6)	0.02 (138)	1.76	89.22
5◆	48.61 (0.2)	36.31 (0.5)	1.10 (2)	1.29 (2)	0.74 (2)	0.02 (26)	0.13 (3)	0.94 (3)	0.09 (28)	1.69	89.23
6◆	47.29 (0.2)	35.33 (0.5)	1.06 (2)	1.27 (2)	0.83 (2)	0.02 (34)	0.10 (4)	1.01 (2)	0.02 (107)	1.69	86.93
7◆	49.22 (0.2)	36.05 (0.5)	1.01 (2)	1.30 (2)	1.10 (2)	0.02 (25)	0.06 (6)	1.25 (2)	0.05 (48)	1.73	90.06
8◆	48.91 (0.2)	35.76 (0.5)	1.01 (2)	1.29 (2)	1.01 (2)	0.01 (51)	0.05 (7)	1.39 (2)	0.07 (34)	1.73	89.50

"-": below detection limit. Parentheses: relative errors %.

TABLE 3. Stoichiometric coefficients of eight studied spots (same as in Table 2) in the cyanoacrylate-affixed LC section based on the formula $(Ca,Mg,Na)_{10-x}[(PO_4)_{6-x}(CO_3)_x](OH)_{2-x}$. The calculated wt% of carbonate and the observed (Ca+Mg+0.5Na)/P molar ratio are included.

#	Formulae	CO_3^{2+} wt%	(Ca+Mg+0.5Na*)/P
1	$(Ca_{8.78}Mg_{0.22}Na_{0.34})[(PO_4)_{5.17}(CO_3)_{0.83}](OH)_{1.17}$	5.4	1.77
2	$(Ca_{8.84}Mg_{0.20}Na_{0.38})[(PO_4)_{5.24}(CO_3)_{0.76}](OH)_{1.24}$	5.0	1.76
3	$(Ca_{8.47}Mg_{0.19}Na_{0.50})[(PO_4)_{4.92}(CO_3)_{1.08}](OH)_{0.92}$	7.1	1.81
4	$(Ca_{8.33}Mg_{0.18}Na_{0.49})[(PO_4)_{4.75}(CO_3)_{1.25}](OH)_{0.75}$	8.4	1.84
5◆	$(Ca_{8.55}Mg_{0.31}Na_{0.35})[(PO_4)_{5.04}(CO_3)_{0.96}](OH)_{1.04}$	6.3	1.80
6◆	$(Ca_{8.57}Mg_{0.32}Na_{0.35})[(PO_4)_{5.06}(CO_3)_{0.94}](OH)_{1.06}$	6.1	1.79
7◆	$(Ca_{8.39}Mg_{0.31}Na_{0.32})[(PO_4)_{4.86}(CO_3)_{1.14}](OH)_{0.86}$	7.6	1.82
8◆	$(Ca_{8.38}Mg_{0.30}Na_{0.31})[(PO_4)_{4.84}(CO_3)_{1.16}](OH)_{0.84}$	7.7	1.83

TABLE 4. Compositions (wt%) of the ashed rostrum, lamb femur, elk antler, Acros synthetic OHAP, and NIST 1486 bone meal (for calibration) based on XRF analysis.

	K^+	Ca^{2+}	Na^+	Mg^{2+}	P	Si^{4+}	Al^{3+}	Ti^{4+}	Fe^{3+}	LOI	Atomic Ratio	
											(Ca+Mg+1/2Na)/P	Ca/P
Rostrum	0.01	36.83	1.37	0.53	16.50	0.01	0.02	-	-	4.59	1.83	1.73
Lamb	0.05	37.79	0.80	0.77	17.97	-	0.01	-	-	1.69	1.71	1.63
Elk	0.02	38.58	0.89	0.86	18.10	0.03	0.01	-	-	0.11	1.75	1.65
Acros	0.01	39.19	0.08	0.54	18.23	0.03	0.01	-	0.01	1.11	1.71	1.66
NIST-1486	0.03	26.81	0.49	0.55	12.38	-	-	-	-	31.20	1.76	1.68

"-": below detection limit.

TABLE 5. Carbon analysis of the rostrum (N=2). Carbonate (CO_3^{2-}) and CO_2 were inferred from TIC. All values shown are in wt%.

	TC	TIC	TOC	CO_3^{2-}	CO_2
Rostrum	2.49±0.00	1.57±0.04	0.91±0.04	7.88±0.22	5.76±0.15

TABLE 6. List of three calculated formulae of bioapatite in the rostrum.

#	Formula	Techniques	Description
1	$(Ca_{8.54}Mg_{0.25}Na_{0.38})[(PO_4)_{4.99}(CO_3)_{1.01}](OH)_{0.99}$	EMP	Analyses of hypermineralized and organic-richer areas in unprocessed rostrum
2	$(Ca_{8.61}Mg_{0.20}Na_{0.42})[(PO_4)_{5.02}(CO_3)_{0.98}](OH)_{1.02}$	EMP	Analyses only of mineral-dominated areas in unprocessed rostrum
3	$(Ca_{8.40}Mg_{0.20}Na_{0.54})[(PO_4)_{4.87}(CO_3)_{1.13}]\ (OH)_{0.87}$	XRF	Bulk analysis of ashed rostrum